ACS Sustainable Chemistry & Engineering

Research Article

Isotopic Studies for Tracking Biogenic Carbon during Co-processing of Biomass and Vacuum Gas Oil

Calvin Mukarakate,* Kellene Orton, Yeonjoon Kim, Stefano Dell'Orco, Carrie A. Farberow, Seonah Kim, Michael J. Watson, Robert M. Baldwin, and Kimberly A. Magrini

Read Online

ACCESS | Metrics & More | Article Recommendations | Supporting Information

ABSTRACT: Co-processing bio-oils with petroleum-derived feeds in the existing multitrillion dollar refining and distribution infrastructure is an attractive option for introducing renewable energy into the fuels marketplace. Considerable research on co-processing bio-oils and vacuum gas oil (VGO) in fluid catalytic cracking units (FCC) using equilibrium catalysts (E-Cats) demonstrated that biomass-derived molecules decreased activity of and increased carbon laydown on E-Cat. In this work, ^{13}C-labeled biomass was co-processed with VGO using either an E-Cat or a proprietary zeolite Johnson Matthey catalyst (CP758), which is optimzed for upgrading biomass vapors in a riser reactor, to evaluate the fate of biogenic carbon in FCC products. The results from both catalysts indicate that biogenic carbon was incorporated into alkenes and aromatic hydrocarbons. While no biogenic carbon was found in linear alkanes, it was observed in cycloalkanes during experiments with E-Cat but not with CP758. All produced CO_2 was biogenic as was most of the carbon laydown on the catalysts. Several partially deoxygenated biomass compounds, such as alkylphenols and benzofurans, unexpectedly contained small amounts of carbon from VGO. Although this study was conducted with labeled biomass and not bio-oil, it provides insights to reaction mechanisms for co-processing bio-oil and VGO in an FCC, which is required to develop catalysts that efficiently convert bio-oil components during FCC co-processing. This work also demonstrates that comprehensive catalyst development utilizing both biomass- and fossil-derived feeds is required to maximize the incorporation of biogenic carbon into transportation fuels.

KEYWORDS: Co-processing, Bio-oils, Fluid catalytic cracking, Biogenic carbon, ^{13}C tracking, Mass spectroscopy
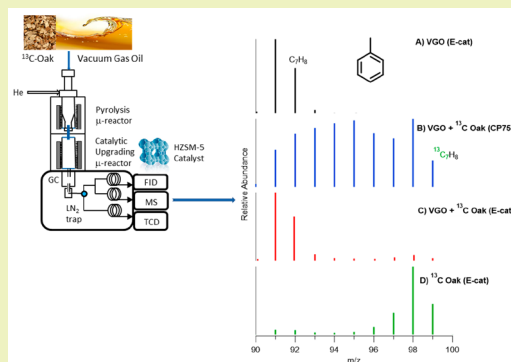
INTRODUCTION

Recently the United States Department of Energy estimated that >1 billion tonnes of biomass can be sustainably harvested each year without impacting land use for farming and wildlife. This renewable resource can be used to supplement approximately 30% of U.S. 2017 consumption of petroleum-derived energy.[1,2] Thus, efforts are underway to develop technologies for converting biomass into fuels and chemicals. Thermochemical processes provide promising approaches for converting biomass into fuels because they use whole biomass (cellulose, hemicellulose, and lignin), produce molecules with carbon chain lengths suitable for fuels, and do not require costly biomass pretreatment. For example, biomass fast pyrolysis produces high yields of bio-oils (up to 75%)[3] though the produced oils contain various oxygen functionalities that cause it to be acidic, unstable, and immiscible with petroleum-derived fuels; these properties are well-documented in the literature.[3-8] Therefore, several approaches are being developed to reduce oxygenated functional groups in bio-oil to improve its quality. One approach integrates catalytic fast pyrolysis of biomass with hydrotreating (CFP−HT) of the

upgraded bio-oils to produce fuel blendstocks.[9-11] Another approach integrates hydropyrolysis and hydroconversion processes (IH^2) using pressurized reactors to convert biomass directly into finished fuels.[12] Although CFP−HT and IH^2 processes produce hydrocarbon fuels with negligible oxygen content, they require stand-alone biorefineries that require extensive capital investments, which increases biofuel and bioproduct production costs.

Co-processing bio-oils with petroleum feeds using the existing petroleum refining infrastructure offers a near-term approach for introducing renewable fuels into the transportation sector without extensive capital investments. The co-processing opportunity is clear as 106 of 136 U.S. refineries have conversion capabilities for heavier distillate fractions.[13] Previous studies investigated co-processing of bio-oils (5—20

wt %) with petroleum-derived feeds using laboratory-scale and pilot-scale systems similar to fluid catalytic cracking (FCC) units.[14−17] Typically, vacuum gas oil (VGO) is upgraded in an FCC unit using an equilibrium catalyst (E-Cat) to produce streams of dry gas (H_2, CO, CO_2, and C_1—C_2), liquefied petroleum gas (LPG; C_3—C_4), gasoline boiling range molecules, light cycle oil (LCO), heavy cycle oil (HCO), and coke. The E-cat, or equilibrium catalyst, is a sample that represents the equilibrium state of the catalyst withdrawn from the FCC reactor as new catalyst is added to maintain catalyst activity. The active component of E-cat is a zeolite combined with other components (filler, binder, and matrix). The co-processing goal is to produce high yields of gasoline and LCO fractions that can be hydrotreated downstream to produce fuel blendstocks. Olefins available in the LPG fraction can also be coupled in a separate reactor to produce fuel range molecules.

Co-processing bio-oil and VGO was found to increase coke yields, gas yields (C_1—C_2, CO and CO_2), liquefied petroleum gas yield, and heavy cycle oil yield compared to VGO only; as a result, the yields for the desirable gasoline and light cycle oil fractions were also reduced.[14,18] Additionally, the H_2 yield decreased during the co-processing experiments and this was attributed to the lower effective hydrogen index of bio-oil leading to hydrogen transfer reactions from VGO. The increase in CO and CO_2 was attributed to deoxygenation of oxygen containing compounds in bio-oils, while the increase in C_1—C_2 was attributed to cracking of light molecules in the bio-oil. The co-processed liquid products contained more aromatic molecules compared to experiments without bio-oils.[14] Trace amounts of oxygenates comprising of simple phenols were also found in liquid products.[15,16,18] The simple phenols were attributed to cracking of lignin methoxyphenols in bio-oils. Surprisingly, small amounts of simple phenols were also observed in effluents from experiments conducted with VGO only.[15] The authors suggested that oxygen from catalyst regeneration was somehow trapped in the pores and reacted with VGO to form phenols.

Accurately measuring biogenic carbon in finished fuels is important to refineries looking to adopt this technology to produce "greener" fuels and to accurately value associated renewable identification numbers (RINs) for carbon accounting and crediting. RINs are credits used for compliance and are the "currency" of the Renewable Fuels Standards Program. Honeywell/UOP and Ensyn have established an alliance for the broad commercialization of refinery co-processing. Under this alliance Honeywell/UOP assists Ensyn in interfacing with refiners and licenses technology to allow refiners to integrate bio-oils into their FCC operations.[19] As highlighted above, co-processing bio-oils and VGO leads to increases in nonfuel fractions, dry gas, LPG, and coke, which suggests that a significant fraction of the biogenic carbon ends up in these nonfuel streams. Fogassy et al.[20] used a carbon-14 (^{14}C) method to discriminate fossil carbon from biogenic carbon, and this method has been effective in determining biogenic carbon in other FCC co-processing product streams. Petrobras[15,16] used the ^{14}C method to measure biogenic carbon in gasoline and LCO fractions, and other FCC products. They demonstrated that the conversion efficiency for biogenic carbon in the desirable gasoline and LCO liquid range products was around 30%. ^{14}C tracking alone does not provide information necessary to develop a fundamental understanding of the chemistry and reaction mechanism(s)

responsible for the incorporation of biogenic carbon into FCC product streams.

The conversion of VGO in FCC using E-Cat occurs through a series of complex reactions comprising thermal cracking of large molecules on the catalyst matrix components to produce small molecules that will fit in the zeolite pores for secondary catalytic cracking. The products observed in FCCs result from cracking, isomerization, hydrogen transfer, transalkylation, cyclization, dealkylation, dehydrogenation, and polymerization reactions.[21−23] Alternatively, biomass conversion is hypothesized to occur on the zeolite catalyst surface to crack sugars and lignin oligomers into small molecules that will reach zeolite pores and react via a common intermediate, "hydrocarbon pool", similar to what is reported for methanol to hydrocarbon processes.[24] The species observed after catalytic upgrading result from deoxygenation, decarboxylation, decarbonylation, dehydration, cracking, coupling, and condensation reactions. The chemistry of either cracking VGO or upgrading bio-oils independently using zeolite-based catalysts is complicated.

In this work, we tracked biogenic carbon during co-processing equal amounts of ^{13}C-labeled oak particles and VGO over an FCC catalyst (E-Cat) and a proprietary zeolite catalyst optimized for biomass upgrading (identified as CP758). These experiments were conducted in a micro-pyrolyzer equipped with a GC-MS/FID system and a quartz annular reactor coupled to an online molecular beam mass spectrometer (MBMS). We demonstrate that biogenic carbon incorporates in olefins, cycloalkanes, and aromatic compounds with boiling ranges in the LPG, gasoline, and LCO fractions. We use theoretical calculations to support proposed reaction mechanisms for cycloalkane formation. Interestingly, we also demonstrate that oxygenates (e.g., simple phenols) found in liquid products are mostly biogenic, but some alkyl groups bonded to oxygenates (e.g., 2,5-dimethylphenol) contain carbon from both biomass and VGO. We acknowledge that bio-oils and not biomass will be the actual feedstock co-processed in refineries and the proportion of VGO to bio-oils envisioned for co-processing in refineries is around 90—95 wt % VGO and 5—10 wt % bio-oil. However, even given these limitations the data from this study provide insight into the fate of biogenic carbon and oxygenates and their impact on co-processing bio-oils with petroleum feeds in an FCC.

■ METHODS

Materials. From IsoLife BV 97% ^{13}C-labeled oak was obtained; VGO was provided by British Petroleum (BP); E-Cat was provided by Equilibrium Catalysts Inc.; and CP758, a ZSM-5-based catalyst, was provided by Johnson Matthey. CP758 was subjected to several reaction and regeneration cycles in a Davison circulating riser (DCR) reactor, upgrading biomass vapors until the effluent compositions were constant. The equilibrated form of CP758 zeolite was used in this work. Table 1 shows the properties of the E-Cat and CP758 catalysts.

Micropyrolyzer−GC-MS System. A micropyrolyzer−GC-MS/FID system was used to identify and quantify the upgraded products from co-processing VGO and oak particles. This system, comprised of a micropyrolyzer (Rx-5030TR, Frontier Laboratories, Japan) coupled to an autosampler (AS-1020E), a microjet cryo-trap (MJT-1030Ex), and a GC-MS/FID/TCD, was used to analyze products from catalytic fast pyrolysis of biomass, and a detailed description about its operation can be found in previous reports.[25−27] Briefly, during the experiments oak, VGO, and catalysts were loaded in deactivated stainless-steel cups. About 300 μg of oak was placed on the bottom of a cup and followed by 300 μg of VGO, and then 10−20 mg of catalyst

Table 1. Catalyst Properties

property	E-Cat	CP758
Na (wt %)	0.2	0.1
0−20 μm (%)	0.0	2.0
0−40 μm (%)	5.0	10
av bulk density (g/cm^3)	0.87	0.72
av particle size (μm)	79	90
surface area (m^2/g)	174	130

was added on top of the samples. Each sample layer was separated by quartz filters. The sample cups were automatically dropped into a furnace set to 550 °C. After reaction, the cracked products were analyzed by a gas chromatograph (GC; 7890B, Agilent Technologies, USA) equipped with a liquid nitrogen trap (−196 °C) and a mass spectrometer (MS; 5977A, Agilent) coupled with an FID. Light gases, such as CH_4 and CO, that passed over the liquid nitrogen trap were analyzed using a GasPro column coupled to a TCD. Heavy compounds on the liquid nitrogen trap were desorbed when the oven temperature increased and then separated by a capillary column (Ultra Alloy-5, Frontier Laboratories, Japan) with a 5% diphenyl/95% dimethylpolysiloxane stationary phase and analyzed by the MS and quantified by the FID. The GC oven was held at 40 °C for 3 min and heated to 300 °C at a ramp rate of 10 °C·min^{-1}. Products recorded on the mass spectrometer were identified using the National Institute of Standards and Technology (NIST) MS library and calibration standards supplied by Accu Standards and consisting of 25 compounds (oxygenates, alkanes, cycloalkanes, and aromatic hydrocarbons). The C_1−C_6 alkane and C_2−C_6 alkene gas standards supplied by Matheson Tri-Gas Inc. were used to identify and quantify light hydrocarbon products. Four different but complementary experiments were conducted in the py-GC-MS/FID system to enable tracking of biogenic carbon incorporation into upgraded products. The first experiment was conducted with unlabeled oak to help identify peaks because the GC-MS cannot assign peaks with isotopes; the second experiment was conducted with ^{13}C-labeled oak, the third with VGO only, and finally the fourth with VGO and ^{13}C-labeled oak mixture.

Horizontal Pyrolizer—MBMS. This reactor system was used to evaluate coke deposits on the catalysts during co-processing oak particles and VGO. The detailed description and application of the horizontal pyrolizer−MBMS (py−MBMS) in studying catalyst coking during catalytic upgrading of biomass was extensively discussed in previous studies.[25−29] Briefly, this system consists of a horizontal quartz annular flow tube reactor coupled with an MBMS. The tube reactor is housed in a four-zone furnace set to 550 °C. Three quartz boats each containing a mixture of 60 mg of VGO and biomass were introduced to the inner tube. The produced vapors and gases were carried by an inner helium flow of 0.4 slm (standard liter per minute) through a 1.5 g fixed bed containing 0.5 g of catalyst mixed with 1 g of inert coarse material to prevent excessive pressure drop across the bed. Helium (4 slm) flowed from the outer tube at the end of the reactor to dilute the cracked products, in order to prevent secondary reactions and meet the flow demands of the MBMS sampling orifice. In addition, 0.04 slm of argon mixed with the helium carrier gas provided a tracer gas to correct drift in the signal resulting from flow changes through the molecular beam inlet. The MBMS monitored real-time signals of the products. After adding three boats of the VGO−biomass mixture, oxygen was added to regenerate the catalyst and monitor the signature of CO_2 evolved during this process. Control experiments were separately conducted with neat VGO and oak to measure CO_2. The co-processing experiments were then repeated, without regenerating the catalyst to collect spent samples for coke quantification by thermogravimetric analysis (TGA). The amount of residual coke deposited on the catalyst generated from the py−MBMS experiment was measured in a TGA Setaram (TN688, SETSYS Evolution) analyzer. The spent catalysts were heated in air at 20 °C min^{-1} from 25 to 780 °C. Two distinct mass loss peaks were observed with the mass loss from 250 to 650 °C attributed to coke,

while that below 250 °C was associated with water and weakly adsorbed species.

Computational Method. The HY zeolite was modeled using a two-layered ONIOM (*n*-layered integrated molecular orbital and molecular mechanics) model,[30] as illustrated in Supporting Information Figure S1. The high-level quantum mechanics (QM) layer was treated with the hybrid wB97xD functional,[31] which includes empirical dispersion, and the 6-311G(d,p) basis set. This layer contains the substrate molecules and 21 tetrahedral sites (21T), which cover the 12-membered ring of the supercage, one Al atom, and one Brønsted acid site. All T sites of HY zeolite are crystallographically equivalent, so one facing the supercage of the high-level layer was selected as the Al site, and additional atoms near the Al site were included in the high-level layer. All four oxygen atoms connected to the Al site are distinct, so the Brønsted site was chosen on the basis of an analysis of relative stability. The low-level molecular mechanics (MM) layer consists of the remaining 435 atoms in the zeolite model cluster, including terminal hydrogen atoms attached with an O−H bond length of 0.96 Å and Si−O−H bond angle of 109.5°. The low-level layer was calculated using the PM6 semiempirical method.[32] During optimization of the geometry, atoms in the high-level layer were allowed to relax, while those in the low-level layer were fixed in their crystallographic positions.

For all of the reactants, intermediates, products, and transition states (TSs), vibrational frequencies were calculated to obtain Gibbs free energies at the given reaction temperature (550 °C), and it was verified that all TSs have one imaginary frequency. Intrinsic reaction coordinate (IRC) calculations[33] were carried out for each TS to find the corresponding reactant and product state. For accurate calculation of adsorption free energies in zeolitic systems, it was assumed that adsorbates retain two-thirds of their translational entropy.[34] All calculations were performed using the Gaussian 16/B.01 program suite.[35] Quasi-harmonic correction to the vibrational entropy was also applied in evaluating Gibbs free energies using the GoodVibes program[36] with a cutoff frequency of 100 cm^{-1}.

RESULTS AND DISCUSSION

Tracking Biogenic Incorporation with GC-MS. The data reported in Figure S2, contained in the Supporting Information, show that cracking neat VGO, ^{13}C oak, and VGO—^{13}C oak mixtures using E-Cat and CP758 resulted in product mixtures with different carbon selectivities for compounds that could be identified by GC-MS. The upgraded products from neat oak are consistent with previous reports for upgrading pyrolysis vapors from different types of biomass and biopolymers over zeolite-based catalysts in micropyrolyzer−GC-MS systems.[26,27,29,37−42] The E-Cat upgraded oak pyrolysis vapors to produce high yields of CO and CO_2 with 56% carbon selectivity to carbon oxides (CO_x) compared to 29% carbon selectivity to CO_x from CP758.

Carbon selectivities to alkenes and aromatic hydrocarbons from E-Cat are low because of the large proportion of zeolite Y in this catalyst, which has been demonstrated to convert biomass vapors into coke.[37,43] The E-Cat cracked neat VGO to produce approximately equal carbon selectivities to alkanes and alkenes compared to CP758, which displayed much higher carbon selectivity to alkenes. The high carbon selectivity to alkenes for CP758 is consistent with previous microscale studies that demonstrated higher alkene selectivities for FCC catalysts doped with increasing proportions of ZSM-5.[44,45] High selectivity to alkenes is attributed to the limited pore volume in ZSM-5 compared to zeolite Y, which makes it difficult to accommodate high molecular weight VGO intermediates. Consequently, more alkenes are then produced via secondary cracking reactions of the VGO intermediates. The aromatic hydrocarbon carbon selectivity from neat VGO

is higher for E-Cat compared to CP758, and we speculate that this was likely due to the production of polycyclic aromatic hydrocarbons (PAHs) from CP758 that were not identified by chromatography. For E-Cat, one-ring aromatic hydrocarbons constituted more than 90% carbon selectivity within the aromatic hydrocarbon fraction compared to 57% carbon selectivity to one-ring aromatic hydrocarbon for CP758, and this observation supports our speculation that CP758 likely produced a higher proportion of PAHs. The cracking of the VGO—^{13}C oak mixtures with both catalysts produced a combination of products representative of contributions from both VGO and oak, and the product selectivities scale with the total carbon percent identified by GC-MS. However, the results shown in Figure S2 do not reveal whether any biogenic carbon was incorporated into VGO products.

The mass spectra of compounds identified by GC-MS in Figure S2 were evaluated to determine the extent to which the two feedstocks reacted independently over the two catalysts. The mass spectra in Figure 1, for toluene identified by GC-MS,
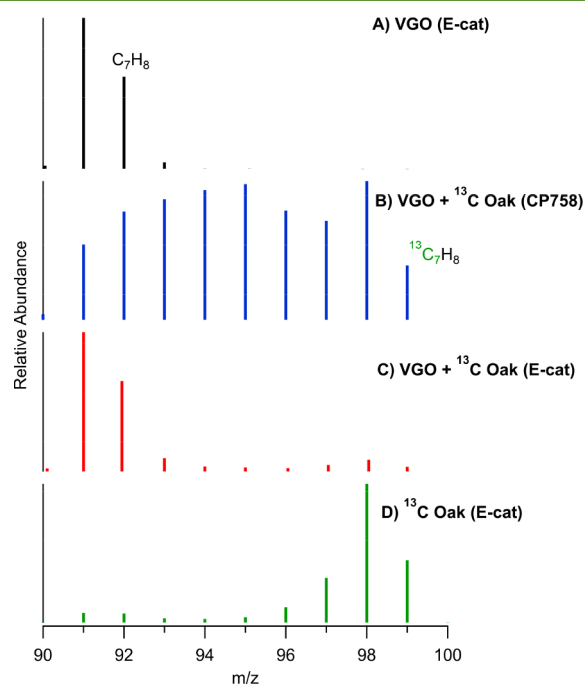
Figure 1. Biogenic carbon incorporation into toluene identified by GC-MS during co-processing of VGO and ^{13}C oak: (A) cracking neat VGO over E-Cat, (B) cracking of VGO—^{13}C oak mixture over CP758, (C) cracking of VGO—^{13}C oak mixture over E-Cat, and (D) cracking neat ^{13}C oak over E-Cat. reaction conditions (VGO, 0.3 mg; oak, 0.3 mg; catalyst, 10 mg; temperature, 550 °C).

show peaks near its parent ion (M), m/z 92, from four separate experiments. Figure 1A, recorded during cracking of neat VGO using E-Cat, shows the parent ion (M) for toluene at m/z 92 and an intense fragment peak at m/z 91 corresponding to the (M − 1) ion and consistent with the toluene mass spectrum observed from cracking VGO over CP758. Figure 1B, recorded when vapors from the VGO—^{13}C oak mixture were cracked over CP758, shows intense peaks ranging from m/z 91 to 99 for toluene. The peaks at m/z 92 (C$_7$H$_8$) and 99 (^{13}C$_7$H$_8$) are attributed to toluene produced from neat VGO and neat ^{13}C oak chemistry, respectively. However, the peaks from m/z 93 (C$_6$^{13}CH$_8$) to 98 (C^{13}C$_7$H$_8$) contain both ^{12}C and ^{13}C from VGO and oak. This is an important result because if VGO and

oak reacted independently over this catalyst, then there should only be intense peaks at m/z 91/92 and 98/99. But we observe scrambling of ^{12}C and ^{13}C carbons indicating that VGO and oak intermediates are interacting with each other and biogenic carbon is getting incorporated into the products from catalytic cracking of VGO and vice versa. Carbon scrambling was previously demonstrated in other isotopic studies on conversion of methanol,[46,47] glucose,[48] cellulose and plastics,[49] and sugar derivatives and hexane,[50] over zeolites. Figure 1C shows that the carbon scrambling from E-Cat was much less pronounced when compared to CP758. As can be seen in Figure 1D, the parent ion (M) for toluene shifted to m/z 99 (corresponding to ^{13}C$_7$H$_8$) when neat ^{13}C oak was used as feed and the corresponding most intense peak shifted to m/z 98 (M − 1) ion. The less intense peaks ($m/z < 97$) in Figure 1D are attributed to the 3% (^{12}C) in the oak sample. The intensities in Figure 1C are different; the oak parent ion (m/z 99) has intensity roughly similar to those of low molecular weight peaks (m/z 94−96) differing from Figure 1D, suggesting that carbon scrambling between the two feeds also occurred over E-Cat. Collectively, these data show that biogenic carbon will be incorporated in toluene during co-processing VGO and bio-oils.

Biogenic carbon incorporation into toluene is enhanced with CP758, and this can be attributed to the high proportion of ZSM-5 additive in this catalyst compared to E-Cat. It has been reported that the conversion of biomass proceeds via a hydrocarbon pool intermediate inside the ZSM-5 pores.[24,48,51,52] We hypothesize that the same hydrocarbon pool chemistry is occurring during the cracking reactions over CP758 because toluene contains equal proportions of ^{12}C from VGO, and ^{13}C from the labeled oak. The intense peak at m/z 98 from CP758 is the analogue toluene (M − 1) fragment from electron impact ionization. The intensities for toluene peaks from CP758, in Figure 1B, are normally distributed, suggesting that most toluene from this catalyst is formed from a common reaction pathway or intermediate.
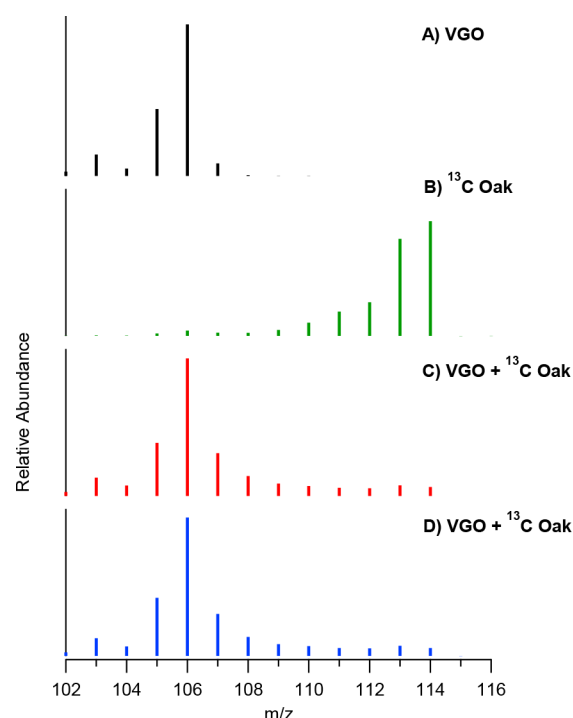
Conversely, the peaks at m/z 91 and 92 for E-Cat, in Figure 1C, are much more intense than the ones containing biogenic carbon, suggesting that toluene observed in this reaction is formed through a different reaction pathway. It is well-known that the catalytic cracking of VGO occurs through a combination of thermal and catalytic cracking of large molecules on the matrix components followed by catalytic cracking of the smaller cracked intermediates on the zeolite active sites.[22] The intense peaks could be attributed to thermal and catalytic cracking of VGO on the catalyst surface, while the low-intensity peaks containing biogenic carbon could be attributed to catalytic cracking on the zeolite Y active sites, where carbon scrambling reactions are possible. The peaks with biogenic carbon (m/z 93−99) in Figure 1C have low intensities due to either lower total acidity of E-Cat or the ineffectiveness of zeolite Y in upgrading biomass pyrolysis products. The latter has been reported in previous biomass CFP studies using zeolite Y, and it has been demonstrated that instead of forming aromatic hydrocarbons this catalyst has the propensity to convert biomass pyrolysis products into coke.[43,53,54] The large proportion of toluene from cracking vapors from VGO−oak mixtures over E-Cat is likely formed from thermal catalytic cracking of VGO on the catalyst surface.

The mass spectra in Figure 2 observed during cracking of the VGO−^{13}C oak mixture over CP758 show that biogenic carbon is also extensively incorporated in xylenes, and the normal
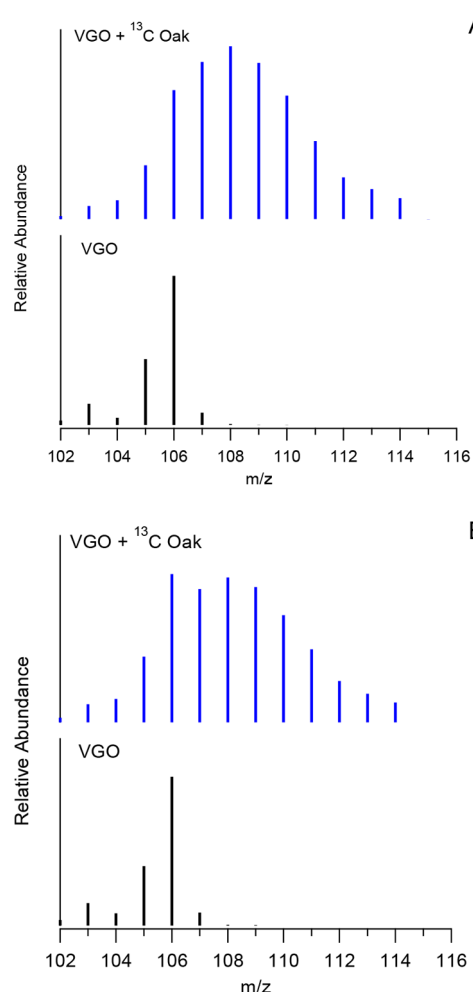
Figure 2. Biogenic carbon incorporation into one-ring aromatic hydrocarbons during co-processing of VGO and ^{13}C-labeled oak over CP758: (A) *p*-xylene and (B) *o*-xylene. Reaction conditions: VGO, 0.3 mg; oak, 0.3 mg; catalyst, 10 mg; temperature, 550 °C.

Figure 3. Biogenic carbon incorporation into xylenes during co-processing of VGO and ^{13}C oak over E-Cat: (A) *p*-xylene from VGO only, (B) *p*-xylene from ^{13}C oak only, (C) *o*-xylene from VGO—^{13}C oak mixture, and (D) *p*-xylene from VGO—^{13}C oak mixture. Reaction conditions: VGO, 0.3 mg; oak, 0.3 mg; catalyst, 10 mg; temperature, 550.

distribution of peaks in *p*-xylene suggests that this compound is formed through a common reaction pathway. Experiments conducted with VGO:^{13}C oak ratio of 2:1 resulted in *p*-xylene with more fossil carbon, while *p*-xylene from a ratio of 1:2 had more contribution from oak (Figure S3). The distribution of peaks for *o*-xylene (Figure 3B) contains two intense peaks (*m/z* 106 and 108), suggesting that this compound is likely formed from two reaction pathways. Most of the *o*-xylene with *m/z* 106 was likely formed from catalytic cracking of VGO on the catalyst mesopores, and most of the remaining peaks were formed from catalytic cracking reactions in the micropores of the catalyst where carbon scrambling can take place via the hydrocarbon pool. This observation can also be partly attributed to the low kinetic diameter of *p*-xylene, which allows it to diffuse easily through the micropores of ZSM-5. The kinetic diameter for *p*-xylene at 5.8 Å is lower than that for *o*-xylene at 6.8 Å, but similar to that for toluene at 5.8 Å.[55] As a result, the amounts of *p*-xylene or toluene quantified in our co-processing experiments were almost eight times higher than *o*-xylene. Bu et al.[56,57] recently used molecular dynamics simulations to demonstrate that molecules with low kinetic diameters have higher diffusion coefficients, and thus can easily escape catalyst micropores before reacting further into PAH and/or eventually coke.

Conversely, Figure 3 shows that biogenic carbon is also incorporated into *o*- and *p*-xylenes (C_8H_{10}) from cracking the VGO—oak mixture with E-Cat. The peaks for biogenic carbon have low intensities, suggesting a modest incorporation of ^{13}C, and they follow the same pattern regardless of the structural differences between the two xylenes. The same mass spectral pattern was also observed for ethylbenzene in the same experiment. This is not surprising because zeolite Y has large pores (7.4 × 7.4 Å), which allow these molecules to diffuse out with similar rates.[55] The intensities for xylene peaks with biogenic carbon are low due to the ineffectiveness of zeolite Y to upgrade biomass-derived molecules into one-ring aromatic hydrocarbons (see Figure S2A).[37,43]

The one-ring aromatic hydrocarbons observed from both E-Cat and CP758 boil in the gasoline range, indicating that biogenic carbon is incorporated in the gasoline fraction during co-processing experiments. This observation agrees with a previous report that demonstrated biogenic carbon incorporation into gasoline liquid effluent using ^{14}C isotopic analysis.[16]

Alkenes and Cycloalkanes. Biogenic carbon also incorporated into alkenes and cycloalkanes. Figure 4 shows mass spectra focused around the parent ion for propylene (*m/z* 42). As shown in Figure 4A, cracking neat VGO produces propylene with the parent peak at *m/z* 42 (C_3H_6), with additional peaks at *m/z* < 42 corresponding to its fragment ions. Other higher molecular weight peaks were observed during cracking of VGO—^{13}C oak mixtures using CP758 (Figure 4B) and E-Cat (Figure 4C), suggesting that the peaks at *m/z* 43, 44, and 45 contain both ^{12}C and ^{13}C $(^{13}C_1{}^{12}C_2H_6,$ $^{13}C_2{}^{12}C_1H_6,$ and $^{13}C_3H_6)$. The parent peak and corresponding fragment ions were shifted to high molecular weight when neat
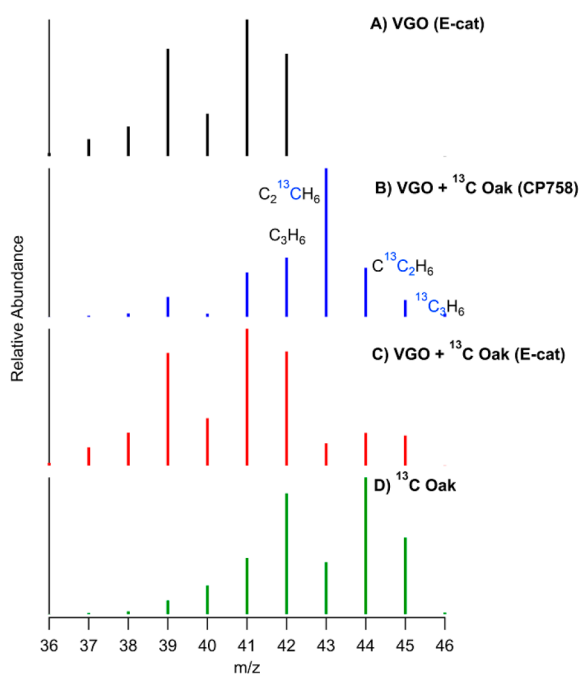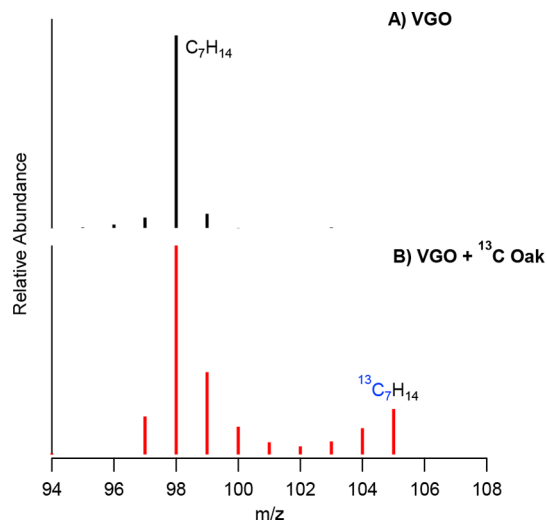
Figure 4. Biogenic carbon incorporation into propylene during co-processing of VGO and ^{13}C-labeled oak: (A) VGO cracking over E-Cat, (B) cracking of VGO—^{13}C oak mixture over CP758, (C) cracking of VGO—^{13}C Oak mixture over E-Cat, and (D) cracking of oak over E-Cat. Reaction conditions: VGO, 0.3 mg; oak, 0.3 mg; catalyst, 10 mg; temperature, 550 °C.

^{13}C oak was the feed (Figure 4D vs Figure 4A), and the intensities of these peaks are different from those recorded with VGO—^{13}C oak mixtures (Figure 4B,C). Figure S4 shows that biogenic carbon also incorporated into methylpropene. The C_2–C_4 alkenes are produced from catalytic cracking on zeolite Y for E-Cat and via the hydrocarbon pool for CP758 and were observed when neat VGO and neat oak were fed separately into the micropyrolyzer. However, high molecular weight alkenes (>C4) were observed only from neat VGO and not from neat oak. Analysis of mass spectra of some higher alkenes from the VGO—^{13}C oak mixture showed additional weak peaks near the parent ions. For example, the mass spectra in Figure 5 for one of these higher olefins (2-pentene, m/z 70) shows the peaks at m/z 72 ($C_3^{13}C_2H_{10}$), 73 ($C_2^{13}C_3H_{10}$), 74 ($C_1^{13}C_4H_{10}$), and 75 ($^{13}C_5H_{10}$), though very weak, providing evidence for incorporation of biogenic carbon into higher olefins using both catalysts. The intensities of peaks containing biogenic carbon decreased with increasing molecular weight of alkenes. We hypothesize that the higher alkenes containing biogenic carbon were formed from coupling of biogenic C_2–C_4 alkenes and VGO alkenes. The results indicate that biogenic carbon is incorporated into alkenes that boil in the LPG (C_2–C_4) and gasoline ($\geq C_5$) ranges.

Cycloalkanes (e.g. methylcyclohexane) were observed from cracking VGO only over E-Cat and CP758; no cycloalkanes were observed when just oak vapors were upgraded over the same catalysts. Figure 6 shows mass spectra around the parent ion for methylcyclohexane, m/z 98. As shown in Figure 6A, the parent ion for methylcyclohexane was observed at m/z 98 when VGO was the feed. Additional weak peaks at m/z 100 ($C_5^{13}C_2H_{14}$), 101 ($C_4^{13}C_3H_{14}$), 102 ($C_3^{13}C_4H_{14}$), 103 ($C_2^{13}C_5H_{14}$), 104 ($C^{13}C_6H_{14}$), and 105 ($^{13}C_7H_{14}$) were observed when VGO was cracked over E-Cat in the presence
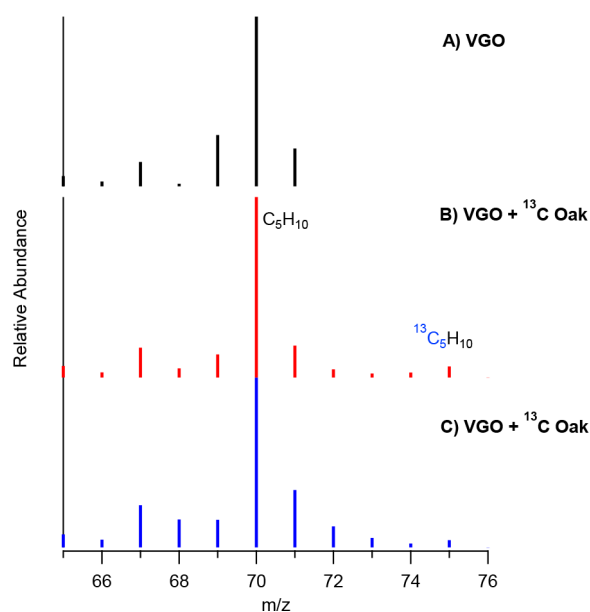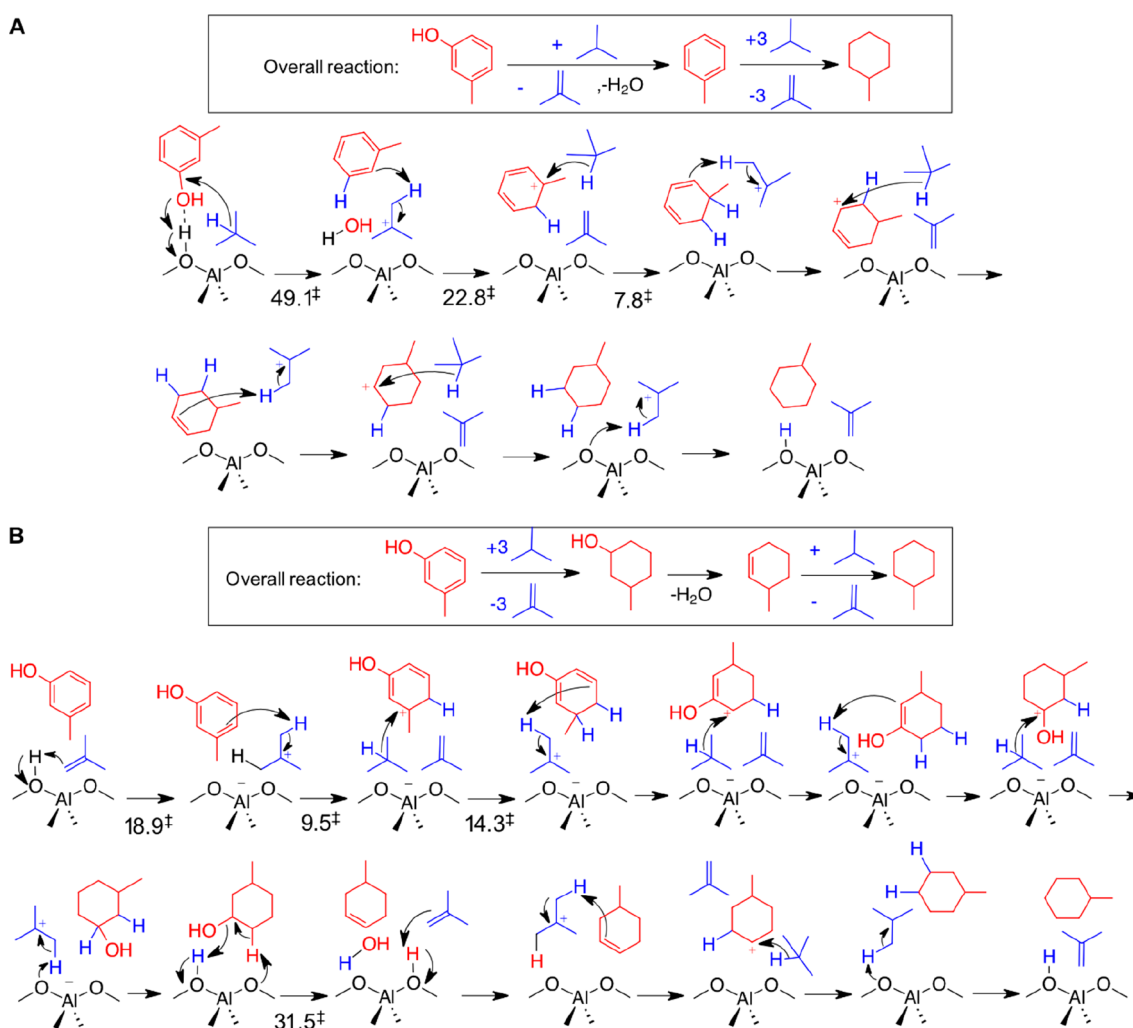

Figure 5. Biogenic carbon incorporation into 2-pentene during co-processing of VGO and ^{13}C-labeled oak: (A) VGO cracking over E-Cat, (B) cracking of VGO—^{13}C oak mixture over E-Cat, and (C) cracking of VGO—^{13}C oak mixture over CP758. Reaction conditions: VGO, 0.3 mg; oak, 0.3 mg; catalyst, 10 mg; temperature, 550 °C.

Figure 6. Biogenic carbon incorporation into methylcyclohexane during co-processing of VGO and ^{13}C-labeled oak: (A) VGO cracking over E-Cat and (B) cracking of VGO—^{13}C oak mixture over E-Cat. Reaction conditions: VGO, 0.3 mg; oak, 0.3 mg; catalyst, 10 mg; temperature, 550 °C.

of oak, suggesting that biogenic carbon was incorporated in cycloalkanes. However, these same peaks were not observed when the mixture was cracked using CP758.

Another surprising observation was the appearance of the peak at m/z 105 for pure ^{13}C methylcyclohexane even though this was not observed when oak was the only feed. Since cycloalkanes and alkenes have the same general formula (C_nH_{2n}), then perhaps this compound could be due to C_7 alkenes. Figure S5 shows the entire mass spectra for methylcyclohexane, including its fragmentation peaks. The most intense fragment peak at m/z 83 (C_6H_{11}) formed after cleavage of a methyl group from the parent ion provides

F

Pursuant to the DOE Public Access Plan, this document represents the authors' peer-reviewed, accepted manuscript.
The published version of the article is available from the relevant publisher.

ACS Sustainable Chemistry & Engineering   pubs.acs.org/journal/ascecg   Research Article

Figure 7. Proposed reaction mechanisms for *m*-cresol conversion to methylcyclohexane. The values indicate the activation energy barriers (kcal mol^{-1}) using the ONIOM (wb97xd:6-311G(d,p):PM6) model at 550 °C. (A) Dehydration to toluene followed by hydride transfer steps and hydrogenation or (B) methylcyclohexanol formation through hydride transfer steps followed by dehydration and hydrogenation reactions. The bio-oil, VGO substrate molecules, and the catalyst are shown in red, blue, and black, respectively. Activation free energy values for all hydride transfer steps have not been calculated, as we assume a similar mechanism with similar barriers to the previous hydride transfer steps.

definitive evidence that this compound was indeed methyl-cyclohexane, and this peak is weaker than the other fragment peaks for linear and branched C_7 alkenes. The m/z 83 fragment also contains additional weak peaks at m/z 84 ($C_5{}^{13}CH_{11}$), 85 ($C_4{}^{13}C_2H_{11}$), 86 ($C_3{}^{13}C_3H_{11}$), 87 ($C_2{}^{13}C_4H_{11}$), 88 ($C^{13}C_5H_{11}$), and 89 ($^{13}C_6H_{11}$) corresponding to addition of ^{13}C to the ring. The assignment for methylcyclohexane was also confirmed with a calibration standard. Similar peak distributions were also observed for cyclopentane and alkylcyclopentanes, and cyclohexane and alkylcyclohexanes. Collectively, these data suggest that cyclo-alkanes observed from E-Cat are likely formed from coupling and cyclization of alkenes, while those from CP758 are formed from VGO primary cracking reactions.

An alternative possible explanation for the presence of pure ^{13}C methylcyclohexane (m/z 105) formed from the VGO$-^{13}C$ oak mixture over E-cat is that hydrocarbons present in the VGO enable hydrogenation through hydride transfer and subsequent deoxygenation of biogenic substituted phenols. To explore this hypothesis, we computationally investigated pathways for conversion of phenolic compounds in bio-oil into methylcyclohexane. *m*-Cresol was used as a model

phenolic compound for ^{13}C-labeled oak, and isobutane/isobutene was used as hydride donor/acceptor molecule derived from VGO. Formation of methylcyclohexane from *m*-cresol can occur via two pathways: dehydration of *m*-cresol followed by consecutive hydride transfer steps (Figure 7A), or hydride transfer followed by dehydration and then additional hydride transfer reactions to produce the saturated methyl-cyclohexane product (Figure 7B). It should be noted that no ^{12}C from VGO is introduced into the methylcyclohexane product in these two reaction pathways and thus the resulting methylcyclohexane contains only ^{13}C biogenic carbon from the phenolic reactant. The former pathway (Figure 7A) involves a high free energy barrier of dehydration (49.5 kcal mol^{-1}) to form toluene, which is consistent with only a small signal for carbon-scrambled toluene observed during co-processing over E-cat (Figure 1C). Alternatively, the latter pathway (Figure 7B) involves low-barrier hydride transfer steps (14−19 kcal mol^{-1}) followed by a dehydration free energy barrier for 3-methylcyclohexanol of only 31.5 kcal mol^{-1}. Thus, deoxyge-nation of phenolics from the bio-oil is likely enabled by initial hydrogenation of these species through hydride transfer from hydrocarbons in the VGO. In summary, biogenic carbon is

Pursuant to the DOE Public Access Plan, this document represents the authors' peer-reviewed, accepted manuscript.
The published version of the article is available from the relevant publisher.

ACS Sustainable Chemistry & Engineering   pubs.acs.org/journal/ascecg   Research Article

incorporated into cycloalkanes during co-processing of VGO and bio-oil using E-Cat, and the cycloalkanes with carbon number > C5 boil in the gasoline fuel range.
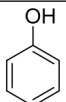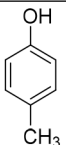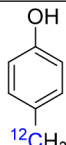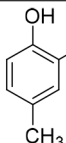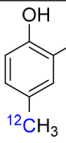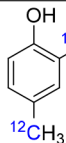
Carbon Oxides and Alkanes. No evidence for carbon scrambling was observed in carbon oxides and linear and branched alkanes during the VGO—^{13}C oak mixture experiments. The deoxygenation of biomass-derived molecules has been reported to occur through decarbonylation, decarboxylation, and dehydration reactions.[26,29] Our results show that the carbon oxides (CO and CO_2) were entirely biogenic, indicating that oxygen removal during catalytic cracking of the VGO−^{13}C-oak mixture takes place exclusively with loss of biogenic carbon. Figure S6A shows the mass spectrum recorded for CO_2 with an intense peak at m/z 45 from $^{13}CO_2$. A small peak at m/z 44 is attributed to background peaks in the GC-MS or the 3% ^{12}C in the sample. Figure S6B also shows that no biogenic carbon incorporated into 3-methylhexane; perhaps this is not surprising because most of the alkanes form by thermal cracking of large VGO molecules on the matrix of the catalyst before moving to the zeolite active sites. The lack of fossil carbon in CO_2 and biogenic carbon in linear and branched chain alkanes was observed over both catalysts. While biogenic carbon loss to carbon oxide gases is undesirable, incorporation of biogenic carbon in light alkenes can provide feedstocks for alkylation reactions producing additional biogenic fuel content or can serve as petrochemical feedstocks for producing polymers with biogenic content.
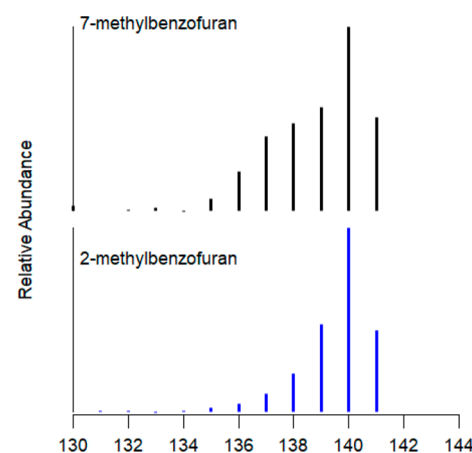
Oxygen Containing Molecules. Most of the biomass-derived oxygenates contained predominately ^{13}C; however, some compounds contained both ^{12}C and ^{13}C. Figure S7A shows mass spectra for phenol recorded from cracking neat ^{13}C oak (upper panel) and VGO—^{13}C oak mixture (lower panel) over CP758 catalyst. The phenol (m/z 100 instead of 94) observed in this work was all biogenic, and there was no evidence for carbon scrambling. This is not surprising since phenol forms from demethoxylation of lignin pyrolysis products,[58] and this reaction does not occur via the same common intermediate (hydrocarbon pool) as olefins and aromatics. Conversely, some low molecular weight peaks compared to the parent ions were observed for 4-methylphenol (m/z 115) in Figure S7B and 2,4-dimethylphenol (m/z 130) in Figure 8. As can be seen in Figure 8, two additional intense peaks are observed next to the parent ion, as well as to the most intense fragment peak at m/z 114 when the mixture was processed in the reactor. Similarly, one additional intense peak is observed next to the parent ion for 4-methylphenol with no additional peaks observed in the fragment ions. Our hypothesis for this observation is that methyl groups ($^{12}CH_3$-) attached to the biogenic phenol backbone contain ^{12}C (Table 2). The parent ions for 2,4-dimethylphenol are at m/z 130 containing just biogenic carbon, 129 consisting of fossil carbon on one of the methyl side groups, and 128 consisting of fossil carbon on both methyl side groups. The presence of fragment ions formed after cleavage of one of the methyl groups in Figure 8 around m/z 114 supports this finding. The methyl groups are produced in the hydrocarbon pool and are coupled with the phenol backbone from oak. This hypothesis is supported by the mass spectra for furan (Figure S7C), and 2-methylbenzo-furan and 7-methylbenzofuran in Figure 9. Furan, like phenol, was also 100% biogenic as expected since this compound is produced from decarbonylation of furfural. The mass spectrum of 7-methylbenzofuran shows several low molecular weight peaks next to the parent peaks when the mixture was processed
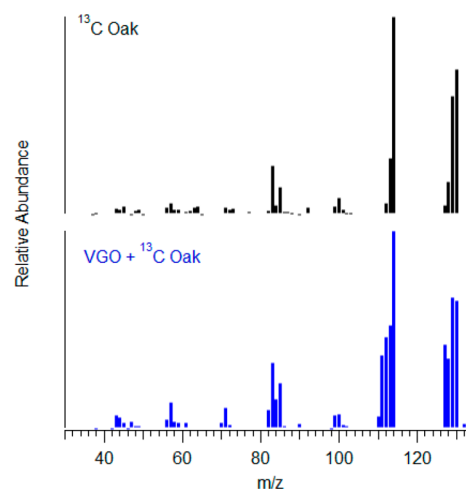
Figure 8. Fossil carbon incorporation into 2,4-dimethylphenol during co-processing of VGO and ^{13}C-labeled oak over CP758. Reaction conditions: VGO, 0.3 mg; oak, 0.3 mg; catalyst, 10 mg; temperature, 550 °C.

Table 2. Simple Phenols Observed during Co-processing VGO and ^{13}C-Labeled Oak over CP758

| Phenols	m/z	Phenols	m/z	Phenols	m/z
OH (phenol)	100	OH, CH3 (4-methylphenol)	115	OH, $^{12}CH_3$ (4-methylphenol)	114
OH, CH3, CH3 (2,4-dimethylphenol)	130	OH, CH3, $^{12}CH_3$ (2,4-dimethylphenol)	129	OH, $^{12}CH_3$, $^{12}CH_3$ (2,4-dimethylphenol)	128

Figure 9. Biogenic carbon incorporation into 7-methylbenzofuran and 2-methylbenzofuran during co-processing of VGO and ^{13}C-labeled oak over CP758. Reaction conditions: VGO, 0.3 mg; oak, 0.3 mg; catalyst, 10 mg; temperature, 550 °C.

in the reactor and limited scrambling was observed in the mass spectrum for 2-methylbenzofuran. The peaks in Figure 9 can be assigned to $^{13}C_9H_8O$ (m/z 141), $C^{13}C_8H_8O$ (m/z 140), $C_2^{13}C_7H_8O$ (m/z 139), $C_3^{13}C_6H_8O$ (m/z 138), $C_4^{13}C_5H_8O$ (m/z 137), and $C_5^{13}C_4H_8O$ (m/z 136). The 2-methylbenzo-
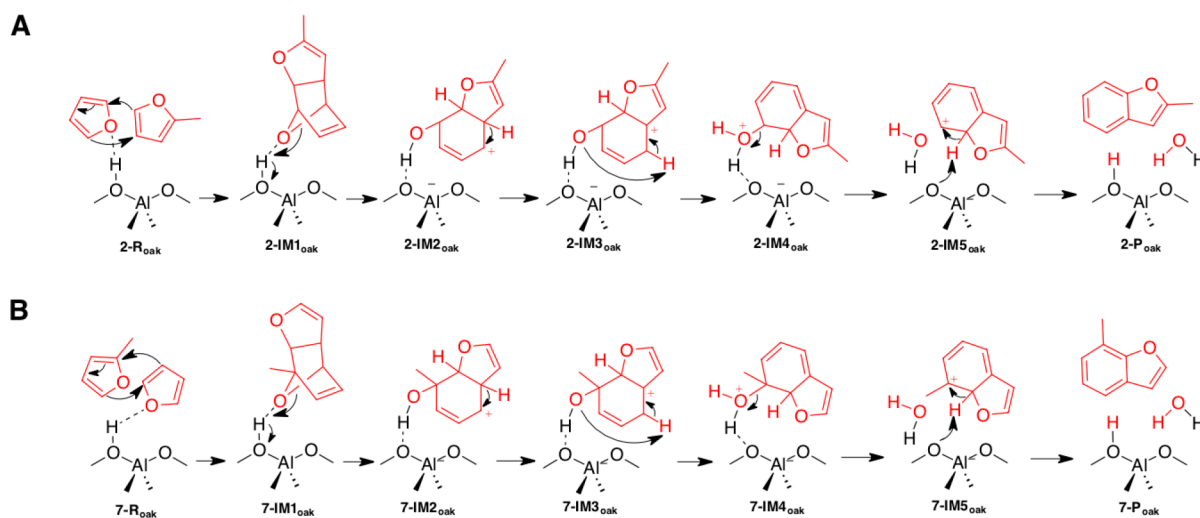
Figure 10. Proposed reaction mechanism for (A) 2-methylbenzofuran and (B) 7-methylbenzofuran formation from biomass-derived (bio) furan and methylfuran. The substrate molecule and the catalyst are shown in red and black, respectively (R, reactant; IM, intermediate; P, products).
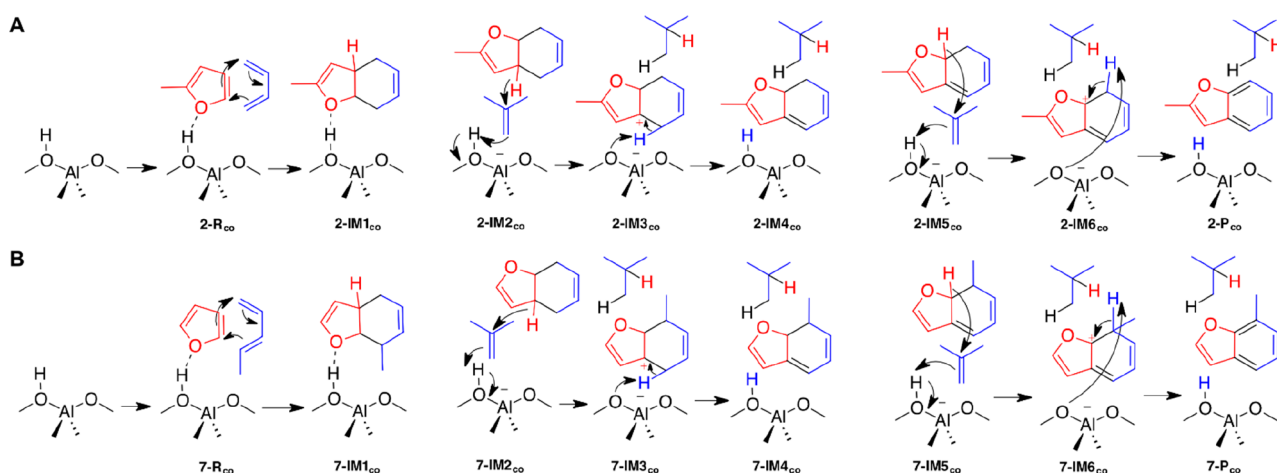
Figure 11. Proposed reaction mechanism for (A) 2-methylbenzofuran and (B) 7-methylbenzofuran formation from bio-derived furans and alkenes derived from fossil or biogenic carbon during co-processing (co). The bio-derived species (furan or methylfuran), alkenes, and the catalyst are shown in red, blue, and black, respectively (R, reactant; IM, intermediate; P, products).

furan and 7-methylbenzofuran with all biogenic carbons (m/z 141) are formed from Diels−Alder reaction between furan and methylfuran. These data suggest that methylbenzofuran peaks with m/z < 141 are likely formed from reactions of furan or alkylfurans from biomass with hydrocarbon precursors available in the hydrocarbon pool to produce alkylbenzofurans. On the basis of the m/z numbers from peaks in Figure 9, we proposed pathways for formation of peaks with both biogenic and VGO carbon (Figures 10 and 11).

As can be seen in Figure 10, the formation of 2-methylbenzofuran initiates with adsorption and Diels−Alder reaction between the two furan molecules (2-R_{oak} → 2-$TS1_{bio}$ → 2-$IM1_{bio}$). The reaction proceeds through protonation and opening of the oxabicyclic ring to produce 2-$IM2_{oak}$ through 2-$TS2_{oak}$. Then the intermediate undergoes two consecutive hydride shifts induced by the carbocation center formed after the ring-opening, via 2-$IM3_{oak}$, leading to the oxonium ion 2-$IM4_{oak}$. Finally, the intermediate is dehydrated to produce 2-methylbenzofuran and regenerate the catalytic site (2-P_{oak}). The 7-methylbenzofuran formation follows a reaction pathway similar to that of 2-methylbenzofuran; furan and 2-methylfuran act as diene and dienophile, respectively, in the formation of 2-

methylbenzofuran, whereas they function in opposite roles during 7-methylbenzofuran formation. The formation of the carbon-scrambled 2-methylbenzofuran and 7-methylbenzofuran can be explained by a Diels−Alder reaction involving reaction of methylfuran or furan with a C_4 or C_5 alkene, respectively (Figure 11). The reaction between 2-methylfuran and butadiene can occur during co-processing for formation of 2-methylbenzofuran with m/z 137 (see Figure 9). This reaction proceeds through adsorption of 2-methylfuran followed by Diels−Alder cycloaddition between butadiene and the adsorbed 2-methylfuran (2-R_{co} → 2-$TS1_{co}$ → 2-$IM1_{co}$). Next, the intermediate loses four hydrogens located at the sp^3 carbons of 2-$IM1_{co}$ through hydride transfer from the substrate molecule to an alkene. Isobutene was chosen as a representative hydride acceptor, and it is introduced into the pore (2-$IM2_{co}$). It can be protonated to form the stable *tert*-butyl cation and receive a hydride from the benzofuran intermediate. These reactions occur simultaneously via a single TS (2-$TS2_{co}$) and lead to the formation of isobutane and the cation intermediate (2-$IM3_{co}$). Subsequently, one neighboring hydrogen is eliminated by deprotonation (2-$IM3_{co}$ → 2-$IM4_{co}$), which terminates the first hydride transfer. The second

transfer occurs in the same manner by introducing another isobutene (2-IM5$_{co}$). This eventually results in the formation of 2-methylbenzofuran (2-P$_{co}$) through 2-TS4$_{co}$, 2-IM6$_{co}$, and 2-TS5$_{co}$.

Formation of 7-methylbenzofuran with m/z 136 follows a similar mechanism with slightly different reactants (pentadiene from the VGO/bio-oil, assumed to contain primarily fossil carbon, and bio-derived furan). The proposed mechanisms shown in Figure 11 can produce methylbenzofurans with other carbon-scrambled mass peaks (m/z 138−140) by considering alkene reactants with varying amounts of biogenic carbon as observed experimentally (Figure 9). Similar reactions of biomass-derived molecules and aromatic precursors in the hydrocarbon pool were demonstrated during reactions of labeled cellulose and aromatic hydrocarbons.[48] The chromatogram peaks for phenols from E-Cat during processing of the VGO—^{13}C oak mixture severely overlapped with hydrocarbons from catalytic cracking of VGO; as such the peak deconvolution program used did not produce pure mass spectra from each component in the overlapped peaks. Phenols and benzofurans observed during co-processing experiments contain small proportions of ^{12}C.

Polyaromatic Hydrocarbons. Additional evidence for reactions of aromatic precursors from the hydrocarbon pool with biomas-derived molecules is highlighted in Figure 12 for experiments with CP758. This figure shows peaks from naphthalene and 2-methylnaphthalene, which are skewed to the left, indicating that the PAHs have a larger proportion of biogenic carbon compared to ^{12}C carbon. This likely happens when the aromatic precursor, already consisting of ^{12}C and ^{13}C available in the hydrocarbon pool (perhaps low kinetic diameter aromatics), reacts with a biomass-derived molecule to form PAHs with a higher proportion of ^{13}C. The mass spectra from both E-Cat and CP758 indicate that PAHs are formed via two different reaction mechanisms. For example, during experiments with E-Cat, most of the naphthalene observed at m/z 128, is likely produced from catalytic cracking on the catalyst surface. The remaining peaks with a combination of ^{12}C and ^{13}C peaks are likely formed from reactions on the active sites of zeolite Y. The distribution of peaks between one- and two-ring aromatics are similar for E-Cat, because of its large pore sizes. The naphthalene produced during experiments with CP758 were mostly produced from the hydrocarbon pool in the micropores of the catalyst because they contain both ^{12}C and ^{13}C, whereas most of this compound at m/z 128 was likely formed in the mesopores of the catalyst. Most PAHs observed from CP758 displayed the same peak distribution, and this suggests that biogenic carbon promotes formation of PAHs, which could eventually lead to coke formation in this catalyst.
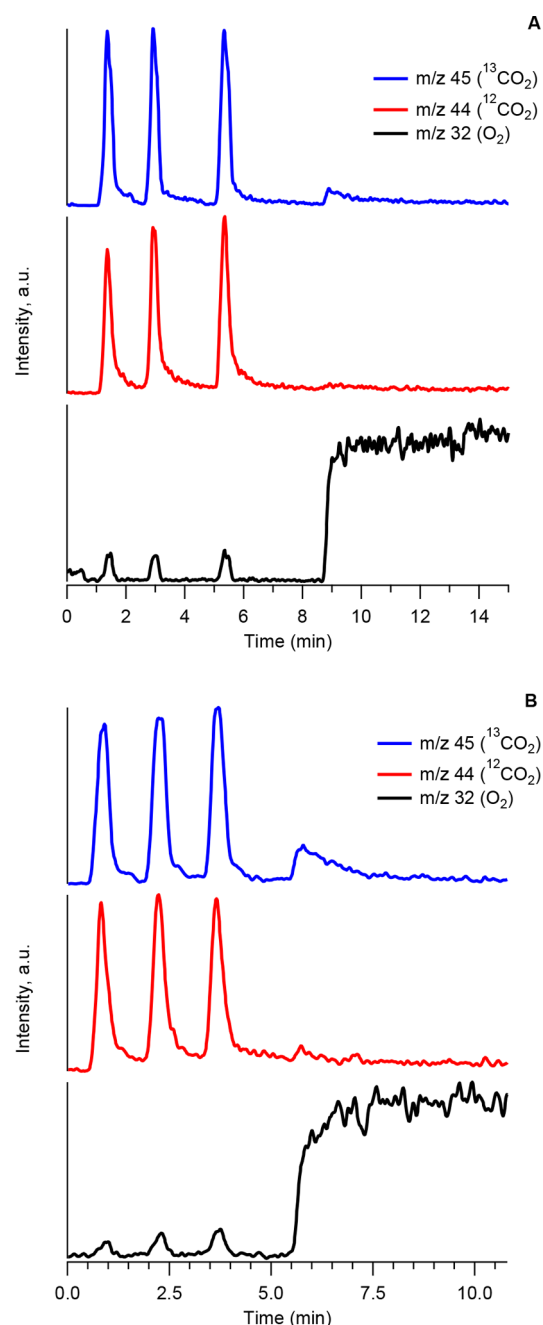
Catalyst Coke Deposits Analyzed with MBMS. Reports show that co-processing bio-oils and VGO results in increased coke deposits on the catalyst.[14,16] In order to identify and demonstrate the source of coke deposition, a series of py−MBMS experiments were conducted in which several VGO—^{13}C oak mixtures were sequentially cracked over a fixed bed containing E-Cat at 550 °C and, after upgrading the mixture, oxygen was added to regenerate the coked catalyst. Figure 13A shows ion signals for selected species generated during sequential catalytic cracking followed by oxidation of the spent catalyst. As shown, the first three pulses contain species separated into m/z 45, 44, and 32, and these are assigned to mixtures of hydrocarbon fragment ions (alkanes
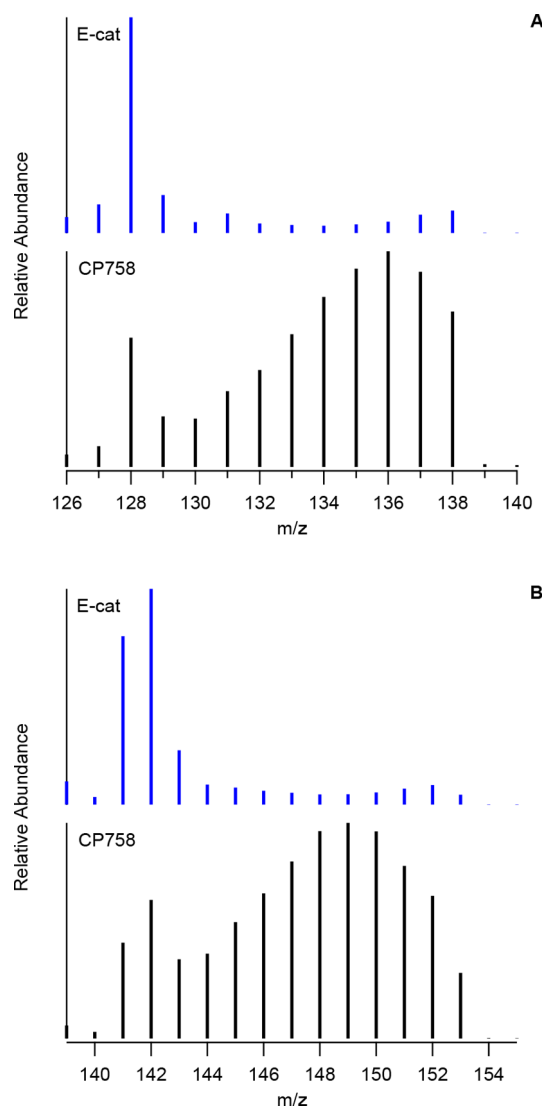
Figure 12. Biogenic carbon incorporation into (A) naphthalene and (B) 2-methylnaphthalene during co-processing of VGO and ^{13}C-labeled oak over CP758. Reaction conditions: VGO, 0.3 mg; oak, 0.3 mg; catalyst, 10 mg; temperature, 550 °C.

and alkenes) plus CO_2 (deoxygenation of biomass oxygenates). Oxygen was added after 9 min to burn off coke deposited on the catalyst. A signal at m/z 45 ($^{13}CO_2$) and not 44 ($^{12}CO_2$) increased rapidly (at about 9 min in Figure 13A) and then decreased gradually indicating that the carbon removed from the catalyst was essentially 100% biogenic. Additional evidence is provided when two similar experiments were conducted separately with VGO and ^{13}C oak. Figure S8A shows that a peak at m/z 45 is produced during regeneration of spent E-Cat after catalytic upgrading of ^{13}C oak. There was no peak observed during regeneration of spent E-Cat after catalytic cracking of VGO, even after loading almost twice the amount of VGO as oak (Figure S8B). Experiments conducted with nonlabeled oak showed a peak at m/z 44 during catalyst regeneration.

These results are not surprising because biomass is hydrogen deficient and as highlighted above zeolite Y has the ability to convert biomass oxygenates into coke. Figure 13B, from a similar experiment with CP758, also shows an intense peak at m/z 45 during catalyst regeneration, indicating that coke

Table 3. Results from Addition of Steam to Oak CFP Using ZSM-5 Performed on the py-MBMS System

sample	water mass loss (mg)	coke mass loss (mg)	% coke on dry coke free basis
CP758	0.13	0.29	0.67
E-Cat	0.045	0.35	0.60

deposited on CP758 was slightly higher than that on zeolite Y. Thus, biomass-derived molecules are responsible for coke buildup during co-processing experiments.

CONCLUSIONS

In this report we demonstrated that when co-processing biomass with VGO, biogenic carbon was observed in both desirable and undesirable FCC product streams using both E-Cat and CP758 catalysts. Biogenic carbon was found in alkenes, cycloalkanes, aromatic hydrocarbons, and coke. There was no biogenic carbon incorporation in linear alkanes, which were mostly formed from thermal cracking of VGO. All CO_2 observed in this work was biogenic and polyaromatic hydrocarbons from CP758 had a higher proportion of biogenic carbon, suggesting that biomass increased coking rates for this catalyst. Conclusive evidence was provided by the intense m/z 45 peak from CO_2 produced while regenerating both spent catalysts. Interestingly, some biomass oxygenates, for example, phenol and furan, contained all ^{13}C, and others, such as alkylbenzofuran and alkylphenols, had ^{12}C from VGO, suggesting reactions of biomass-derived molecules with hydrocarbon precursors on catalyst active sites. Collectively, the results suggest that biogenic carbon incorporation is impacted by catalyst type, composition, and strength of active sites. To this end, comprehensive catalyst development is required to increase biogenic carbon incorporation into conventional fuels without impacting conversion of petroleum feeds. This is different from current research efforts where catalyst development for biomass and petroleum feeds are conducted separately.

ASSOCIATED CONTENT

Supporting Information

The Supporting Information is available free of charge at https://pubs.acs.org/doi/10.1021/acssuschemeng.9b05762.

    HY zeolite cluster model, product selectivity graphs, additional products mass spectra, and coke signature profiles (PDF)

AUTHOR INFORMATION

Corresponding Author

    Calvin Mukarakate — *National Renewable Energy Laboratory, Golden, Colorado 80401-3393, United States;* orcid.org/0000-0002-3919-7977; Email: Calvin.Mukarakate@nrel.gov

Authors

    Kellene Orton — *National Renewable Energy Laboratory, Golden, Colorado 80401-3393, United States*

    Yeonjoon Kim — *National Renewable Energy Laboratory, Golden, Colorado 80401-3393, United States*

    Stefano Dell'Orco — *Department of Industrial Engineering, University of Florence, 50134 Florence, Italy*

    Carrie A. Farberow — *National Renewable Energy Laboratory, Golden, Colorado 80401-3393, United States*

Figure 13. Ion signals of products from co-processing of VGO and ^{13}C oak followed by catalyst oxidative regeneration in the py-MBMS using (A) E-Cat and (B) CP758. Reaction conditions: VGO, 30 mg; oak, 30 mg; per pulse catalyst, 500 mg; temperature, 550 °C.

formed from this catalyst was mostly biogenic; a small peak observed at m/z 44 suggests that coke was also formed from ^{12}C constituent. This is in good agreement with the data for PAHs where the proportion of the ^{13}C increased with each additional aromatic ring. Collectively, these data suggest that coke on E-Cat is formed on the surface of the catalyst. Coke on CP758 was formed in the micropores leading to contribution from the ^{12}C component and, as reported in numerous studies, from condensation of lignin and sugar oligomers on the catalyst surface.[26] The experiments with both catalysts were repeated in order to quantify coke deposits using thermogravimetric analysis. Table 3 shows that the amount of coke

Seonah Kim − *National Renewable Energy Laboratory, Golden, Colorado 80401-3393, United States;* ⦿ orcid.org/0000-0001-9846-7140

Michael J. Watson − *Johnson Matthey Technology Centre, Billingham, Cleveland TS23 1LB, United Kingdom*

Robert M. Baldwin − *National Renewable Energy Laboratory, Golden, Colorado 80401-3393, United States*

Kimberly A. Magrini − *National Renewable Energy Laboratory, Golden, Colorado 80401-3393, United States;* ⦿ orcid.org/0000-0002-0216-7424

Complete contact information is available at:
https://pubs.acs.org/10.1021/acssuschemeng.9b05762

Notes

The authors declare no competing financial interest.

■ REFERENCES

(1) Efroymson, R. A.; Langholtz, M. H.; Johnson, K. E.; Stokes, B. J. *2016 Billion-Ton Report: Advancing Domestic Resources for a Thriving Bioeconomy, Volume 2: Environmental Sustainability Effects of Select Scenerios from Volume 1*; Oak Ridge National Laboratory, U. S. Department of Energy: Oak Ridge, TN, USA, 2016.

(2) Langholtz, M. H.; Stokes, B. J.; Eaton, L. M. *2016 Billion-Ton Report: Advancing Domestic Resorces for a Thriving Bioeconomy, Vol. 1: Economic Avaiability of Feedstocks*; Oak Ridge National Laboratory, U.S. Department of Energy: Oak Ridge, TN, USA, 2016.

(3) Bridgwater, A. V.; Czernik, S.; Diebold, J.; Meier, D.; Oasmaa, A.; Peacocke, C.; Piskorz, J.; Radlein, D. *Fast Pyrolysis of Biomass: A Handbook*; CPL Press: Newbury, U.K., 1999; Vol. 1, pp 1−188.

(4) Bridgwater, A. V., Ed. *Fast Pyrolysis of Biomass: A Handbook Vol. 2*; CPL Press: Newbury, U.K., 2002; Vol. 2, pp 1−424.

(5) Czernik, S.; Bridgwater, A. V. Overview of applications of biomass fast pyrolysis oil. *Energy Fuels* **2004**, *18* (2), 590−598.

(6) Oasmaa, A.; Leppamaki, E.; Koponen, P.; Levander, J.; Tapola, E. *Physical characterisation of biomass-based pyrolysis liquids*; VTT (Technical Research Centre of Finland): Espoo, Finland, 1997; Vol. 306, pp 1−87.

(7) Oasmaa, A.; Peacocke, C. *A guide to physical property characterisation of biomass-derived fast pyrolysis liquids*; VTT (Technical Research Centre of Finland); Espoo, Finland, 2001; Vol. 450, pp 1−102.

(8) Oasmaa, A.; Peacocke, C. *Properties and fuel use of biomass-derived fast pyrolysis liquids. A guide*; VTT (Technical Research Centre of Finland): Espoo, Finland, 2010; Vol. 731, pp 1−134.

(9) Griffin, M. B.; Iisa, K.; Wang, H.; Dutta, A.; Orton, K. A.; French, R. J.; Santosa, D. M.; Wilson, N.; Christensen, E.; Nash, C.; Van Allsburg, K. M.; Baddour, F. G.; Ruddy, D. A.; Tan, E. C. D.; Cai, H.; Mukarakate, C.; Schaidle, J. A. Driving towards cost-competitive biofuels through catalytic fast pyrolysis by rethinking catalyst selection and reactor configuration. *Energy Environ. Sci.* **2018**, *11*, 2904−2918.

(10) Iisa, K.; French, R. J.; Orton, K. A.; Dutta, A.; Schaidle, J. A. Production of low-oxygen bio-oil via ex situ catalytic fast pyrolysis and hydrotreating. *Fuel* **2017**, *207*, 413−422.

(11) Mante, O. D.; Dayton, D. C.; Gabrielsen, J.; Ammitzboll, N. L.; Barbee, D.; Verdier, S.; Wang, K. Integration of catalytic fast pyrolysis and hydroprocessing: a pathway to refinery intermediates and "drop-in" fuels from biomass. *Green Chem.* **2016**, *18* (22), 6123−6135.

(12) Marker, T. L.; Felix, L. G.; Linck, M. B.; Roberts, M. J. Integrated hydropyrolysis and hydroconversion (IH2) for the direct production of gasoline and diesel fuels or blending components from biomass, part 1: Proof of principle testing. *Environ. Prog. Sustainable Energy* **2012**, *31* (2), 191−199.

(13) Freeman, C.; Jones, S.; Padmaperuma, A.; Santosa, M.; Valkenburg, C.; Shin, J. *Initial Assessment of U.S. Refineries for Purposes of Potential Bio-Based Oil Insertions*, PNNL-22432; Pacific Northwest National Laboratory (PNNL): Richaland, WA, USA, 2013.

(14) Lindfors, C.; Paasikallio, V.; Kuoppala, E.; Reinikainen, M.; Oasmaa, A.; Solantausta, Y. Co-processing of dry bio-oil, catalytic pyrolysis oil, and hydrotreated bio-oil in a micro activity test unit. *Energy Fuels* **2015**, *29* (6), 3707−3714.

(15) Pinho, A. d. R.; de Almeida, M. B. B.; Mendes, F. L.; Casavechia, L. C.; Talmadge, M. S.; Kinchin, C. M.; Chum, H. L. Fast pyrolysis oil from pinewood chips co-processing with vacuum gas oil in an FCC unit for second generation fuel production. *Fuel* **2017**, *188*, 462−473.

(16) Pinho, A. d. R.; de Almeida, M. B. B.; Mendes, F. L.; Ximenes, V. L.; Casavechia, L. C. Co-processing raw bio-oil and gasoil in an FCC Unit. *Fuel Process. Technol.* **2015**, *131*, 159−166.

(17) Zacher, A. *Optimizing co-processing of bio-oil in refinery unit operations using a Davison circulating riser (DCR)*; Pacific Northwest National Laboratory (PNNL): Richland, WA, USA, 2015.

(18) Bryden, K.; Weatherbee, G.; Habib, E. T., Jr. Flexible pilot plant technology for evaluation of unconventional feedstocks and processes. *Grace Catal. Technol. Catalagram* **2013**, *113*, 3−21.

(19) Terakado, O.; Yanase, H.; Hirasawa, M. Pyrolysis treatment of waste polyurethane foam in the presence of metallic compounds. *J. Anal. Appl. Pyrolysis* **2014**, *108*, 130−135.

(20) Fogassy, G.; Thegarid, N.; Schuurman, Y.; Mirodatos, C. The fate of bio-carbon in FCC co-processing products. *Green Chem.* **2012**, *14* (5), 1367−1371.

(21) Corma, A.; Orchilles, A. V. Current views on the mechanism of catalytic cracking. *Microporous Mesoporous Mater.* **2000**, *35−36*, 21−30.

(22) Dupain, X.; Makkee, M.; Moulijn, J. A. Optimal conditions in fluid catalytic cracking: A mechanistic approach. *Appl. Catal., A* **2006**, *297* (2), 198−219.

(23) Sadeghbeigi, R. *Fluid Catalytic Cracking Handbook*, 3rd ed.; Elsevier: New York, 2012; pp 1−323.

(24) Carlson, T. R.; Jae, J.; Lin, Y.-C.; Tompsett, G. A.; Huber, G. W. Catalytic fast pyrolysis of glucose with HZSM-5: The combined homogeneous and heterogeneous reactions. *J. Catal.* **2010**, *270* (1), 110−124.

(25) Budhi, S.; Mukarakate, C.; Iisa, K.; Pylypenko, S.; Ciesielski, P. N.; Yung, M. M.; Donohoe, B. S.; Katahira, R.; Nimlos, M. R.; Trewyn, B. G. Molybdenum incorporated mesoporous silica catalyst for production of biofuels and value-added chemicals via catalytic fast pyrolysis. *Green Chem.* **2015**, *17* (5), 3035−3046.

(26) Mukarakate, C.; Zhang, X. D.; Stanton, A. R.; Robichaud, D. J.; Ciesielski, P. N.; Malhotra, K.; Donohoe, B. S.; Gjersing, E.; Evans, R. J.; Heroux, D. S.; Richards, R.; Iisa, K.; Nimlos, M. R. Real-time monitoring of the deactivation of HZSM-5 during upgrading of pine pyrolysis vapors. *Green Chem.* **2014**, *16* (3), 1444−1461.

(27) Xu, M.; Mukarakate, C.; Iisa, K.; Budhi, S.; Menart, M.; Davidson, M.; Robichaud, D. J.; Nimlos, M. R.; Trewyn, B. G.; Richards, R. M. Deactivation of Multilayered MFI Nanosheet Zeolite during Upgrading of Biomass Pyrolysis Vapors. *ACS Sustainable Chem. Eng.* **2017**, *5*, 5477−5484.

Pursuant to the DOE Public Access Plan, this document represents the authors' peer-reviewed, accepted manuscript.
The published version of the article is available from the relevant publisher.

ACS Sustainable Chemistry & Engineering pubs.acs.org/journal/ascecg Research Article

(28) Mukarakate, C.; McBrayer, J. D.; Evans, T. J.; Budhi, S.; Robichaud, D. J.; Iisa, K.; Ten Dam, J.; Watson, M. J.; Baldwin, R. M.; Nimlos, M. R. Catalytic fast pyrolysis of biomass: the reactions of water and aromatic intermediates produces phenols. *Green Chem.* **2015**, *17* (8), 4217−4227.

(29) Mukarakate, C.; Watson, M. J.; ten Dam, J.; Baucherel, X.; Budhi, S.; Yung, M. M.; Ben, H.; Iisa, K.; Baldwin, R. M.; Nimlos, M. R. Upgrading biomass pyrolysis vapors over [small beta]-zeolites: role of silica-to-alumina ratio. *Green Chem.* **2014**, *16*, 4891−4905.

(30) Dapprich, S.; Komaromi, I.; Byun, K. S.; Morokuma, K.; Frisch, M. J. A new ONIOM implementation in Gaussian98. Part I. The calculation of energies, gradients, vibrational frequencies and electric field derivatives1Dedicated to Professor Keiji Morokuma in celebration of his 65th birthday.1. *J. Mol. Struct.: THEOCHEM* **1999**, *461−462*, 1−21.

(31) Chai, J.-D.; Head-Gordon, M. Long-range corrected hybrid density functionals with damped atom-atom dispersion corrections. *Phys. Chem. Chem. Phys.* **2008**, *10* (44), 6615−6620.

(32) Stewart, J. J. P. Optimization of parameters for semiempirical methods V: modification of NDDO approximations and application to 70 elements. *J. Mol. Model.* **2007**, *13* (12), 1173−1213.

(33) Gonzalez, C.; Schlegel, H. B. Reaction path following in mass-weighted internal coordinates. *J. Phys. Chem.* **1990**, *94* (14), 5523−5527.

(34) Paolucci, C.; Verma, A. A.; Bates, S. A.; Kispersky, V. F.; Miller, J. T.; Gounder, R.; Delgass, W. N.; Ribeiro, F. H.; Schneider, W. F. Isolation of the Copper Redox Steps in the Standard Selective Catalytic Reduction on Cu-SSZ-13. *Angew. Chem., Int. Ed.* **2014**, *53* (44), 11828−11833.

(35) Frisch, M. J.; Trucks, G. W.; Schlegel, H. B.; Scuseria, G. E.; Robb, M. A.; Cheeseman, J. R.; Scalmani, G.; Barone, V.; Petersson, G. A.; Nakatsuji, H.; Li, X.; Caricato, M.; Marenich, A. V.; Bloino, J.; Janesko, B. G.; Gomperts, R.; Mennucci, B.; Hratchian, H. P.; Ortiz, J. V.; Izmaylov, A. F.; Sonnenberg, J. L.; Williams; Ding, F.; Lipparini, F.; Egidi, F.; Goings, J.; Peng, B.; Petrone, A.; Henderson, T.; Ranasinghe, D.; Zakrzewski, V. G.; Gao, J.; Rega, N.; Zheng, G.; Liang, W.; Hada, M.; Ehara, M.; Toyota, K.; Fukuda, R.; Hasegawa, J.; Ishida, M.; Nakajima, T.; Honda, Y.; Kitao, O.; Nakai, H.; Vreven, T.; Throssell, K.; Montgomery, J. A., Jr.; Peralta, J. E.; Ogliaro, F.; Bearpark, M. J.; Heyd, J. J.; Brothers, E. N.; Kudin, K. N.; Staroverov, V. N.; Keith, T. A.; Kobayashi, R.; Normand, J.; Raghavachari, K.; Rendell, A. P.; Burant, J. C.; Iyengar, S. S.; Tomasi, J.; Cossi, M.; Millam, J. M.; Klene, M.; Adamo, C.; Cammi, R.; Ochterski, J. W.; Martin, R. L.; Morokuma, K.; Farkas, O.; Foresman, J. B.; Fox, D. J. *Gaussian 16*, Rev. B.01; Wallingford, CT, USA, 2016.

(36) Funes-Ardoiz, I.; Paton, R. S. *Good Vibes*, software; 2017.

(37) Carlson, T. R.; Vispute, T. R.; Huber, G. W. Green gasoline by catalytic fast pyrolysis of solid biomass derived compounds. *ChemSusChem* **2008**, *1* (5), 397−400.

(38) Evans, R. J.; Milne, T. A., Molecular-Beam, Mass-Spectrometric Studies of Wood Vapor and Model Compounds over an HZSM-5 Catalyst. In *Pyrolysis Oils from Biomass*; Soltes, E. J., Milne, T. A., Eds.; ACS Symposium Series, Vol. 376; American Chemical Society: Washington, DC, USA, 1988; Chapter 26, pp 311−327, DOI: 10.1021/bk-1988-0376.ch026.

(39) French, R.; Czernik, S. Catalytic pyrolysis of biomass for biofuels production. *Fuel Process. Technol.* **2010**, *91* (1), 25−32.

(40) Mullen, C. A.; Boateng, A. A.; Mihalcik, D. J.; Goldberg, N. M. Catalytic Fast Pyrolysis of White Oak Wood in a Bubbling Fluidized Bed. *Energy Fuels* **2011**, *25* (11), 5444−5451.

(41) Wang, K.; Johnston, P. A.; Brown, R. C. Comparison of in-situ and ex-situ catalytic pyrolysis in a micro-reactor system. *Bioresour. Technol.* **2014**, *173*, 124−131.

(42) Wang, K.; Kim, K. H.; Brown, R. C. Catalytic pyrolysis of individual components of lignocellulosic biomass. *Green Chem.* **2014**, *16*, 727−735.

(43) Carlson, T. R.; Tompsett, G. A.; Conner, W. C.; Huber, G. W. Aromatic Production from Catalytic Fast Pyrolysis of Biomass-Derived Feedstocks. *Top. Catal.* **2009**, *52* (3), 241−252.

(44) Ishihara, A.; Kimura, K.; Hashimoto, T.; Nasu, H. Catalytic cracking of VGO by zeolite-kaolin mixed catalysts using curie point pyrolyzer. *J. Jpn. Pet. Inst.* **2015**, *58* (3), 169−175.

(45) Ishihara, A.; Kimura, K.; Owaki, A.; Inui, K.; Hashimoto, T.; Nasu, H. Catalytic cracking of VGO by hierarchical ZSM-5 zeolite containing mesoporous silica-aluminas using a Curie point pyrolyzer. *Catal. Commun.* **2012**, *28*, 163−167.

(46) Bjørgen, M.; Svelle, S.; Joensen, F.; Nerlov, J.; Kolboe, S.; Bonino, F.; Palumbo, L.; Bordiga, S.; Olsbye, U. Conversion of methanol to hydrocarbons over zeolite H-ZSM-5: On the origin of the olefinic species. *J. Catal.* **2007**, *249* (2), 195−207.

(47) Haw, J. F.; Song, W.; Marcus, D. M.; Nicholas, J. B. The Mechanism of Methanol to Hydrocarbon Catalysis. *Acc. Chem. Res.* **2003**, *36* (5), 317−326.

(48) Carlson, T. R.; Jae, J.; Huber, G. W. Mechanistic Insights from Isotopic Studies of Glucose Conversion to Aromatics Over ZSM-5. *ChemCatChem* **2009**, *1* (1), 107−110.

(49) Dorado, C.; Mullen, C. A.; Boateng, A. A. Origin of carbon in aromatic and olefin products derived from HZSM-5 catalyzed co-pyrolysis of cellulose and plastics via isotopic labeling. *Appl. Catal., B* **2015**, *162*, 338−345.

(50) Batalha, N.; Pinto, J.; Ferreira, H.; Baptista, D. C.; Miranda, L. S. M.; Pereira, M. M. Biohydrocarbons Production under Standard Refinery Conditions by means of a Representative Ketal Compound of Biocrude. *Energy Technol.* **2017**, *5* (3), 428−441.

(51) Xu, M.; Mukarakate, C.; Robichaud, D. J.; Nimlos, M. R.; Richards, R. M.; Trewyn, B. G. Elucidating Zeolite Deactivation Mechanisms during Biomass Catalytic Fast Pyrolysis from Model Reactions and Zeolite Syntheses. *Top. Catal.* **2016**, *59* (1), 73−85.

(52) Zhang, H.; Carlson, T. R.; Xiao, R.; Huber, G. W. Catalytic fast pyrolysis of wood and alcohol mixtures in a fluidized bed reactor. *Green Chem.* **2012**, *14* (1), 98−110.

(53) Lappas, A. A.; Samolada, M. C.; Iatridis, D. K.; Voutetakis, S. S.; Vasalos, I. A. Biomass pyrolysis in a circulating fluid bed reactor for the production of fuels and chemicals. *Fuel* **2002**, *81* (16), 2087−2095.

(54) Aho, A.; Kumar, N.; Lashkul, A. V.; Eranen, K.; Ziolek, M.; Decyk, P.; Salmi, T.; Holmbom, B.; Hupa, M.; Murzin, D. Y. Catalytic upgrading of woody biomass derived pyrolysis vapours over iron modified zeolites in a dual-fluidized bed reactor. *Fuel* **2010**, *89* (8), 1992−2000.

(55) Jae, J.; Tompsett, G. A.; Foster, A. J.; Hammond, K. D.; Auerbach, S. M.; Lobo, R. F.; Huber, G. W. Investigation into the shape selectivity of zeolite catalysts for biomass conversion. *J. Catal.* **2011**, *279* (2), 257−268.

(56) Bu, L.; Nimlos, M. R.; Robichaud, D. J.; Kim, S. Diffusion of aromatic hydrocarbons in hierarchical mesoporous H-ZSM-5 zeolite. *Catal. Today* **2018**, *312*, 73−81.

(57) Bu, L.; Nimlos, M. R.; Robichaud, D. J.; Kim, S. Diffusion of Biomass Pyrolysis Products in H-ZSM-5 by Molecular Dynamics Simulations. *J. Phys. Chem. C* **2017**, *121* (1), 500−510.

(58) Stanton, A. R.; Iisa, K.; Mukarakate, C.; Nimlos, M. R. Role of biopolymers in the deactivation of ZSM-5 during catalytic fast pyrolysis of biomass. *ACS Sustainable Chem. Eng.* **2018**, *6*, 10030−10038.